ELSEVIER

Available online at www.sciencedirect.com
SCIENCE DIRECT®

Geoderma xx (2003) xxx–xxx

GEODERMA

www.elsevier.com/locate/geoderma

Inferring flow types from dye patterns in macroporous soils

Markus Weiler*, Hannes Flühler

Department of Forest Engineering, Oregon State University, Corvallis, OR, 97331-5706, USA

Received 25 February 2003; received in revised form 14 August 2003; accepted 29 August 2003

Abstract

In this study, we exploit dye patterns to identify flow types in macroporous soils as a step forward from using dye patterns simply as qualitative pictures that illustrate preferential flow. Dye tracer experiments at different irrigation rates and initial soil moisture conditions were carried out on three hillslope sites. Several vertical and horizontal soil sections were prepared after each experiment to analyze the patterns of the dye tracer Brilliant Blue FCF. Photographs of the soil sections were processed by image analysis to discriminate between stained and unstained areas and to classify stained areas into three classes of dye concentration. The images of the vertical sections were first analyzed according to conventional approaches (e.g., dye coverage). Then, a new approach was developed using the extent and distribution of the stained objects to classify flow into five types, two of these flow types occur only in the soil matrix, and three of them are related to the degrees of water flow between macropores and soil matrix (interaction). From horizontal sections, the macropore distribution was classified and, in combination with the dye pattern, the interaction quantified based on statistical description of the spatial relationship between macropores and stained areas. Categorized flow type profiles showed a logical sequence in each of our experiments, and we think the concepts will have broad application in soil science and infiltration research to compare the infiltration regimes of soils.

Keywords: Dye pattern; Unsaturated zone; Image analysis; Flow types; Macropore flow

1. Introduction

Dye tracing for staining flow pathways has become an established way to demonstrate the occurrence of preferential flow in soils (Flury et al., 1994; Ghodrati and Jury, 1990; Peterson et al., 1997; van Ommen et al., 1989). However, using dye patterns simply as nice qualitative pictures that illustrate preferential flow in soils is not sufficient, as we think they can more efficiently be used to quantify and compare flow processes in soils. The dye tracer studies commonly add a dye tracer to water sprinkled on soil, so that the resulting infiltration pattern can be visualized at excavated soil sections. Various tracers have been used, including the strongly sorbing Methylene Blue (Bouma et al., 1977), the more moderate Acid Red 1 (Ghodrati and Jury, 1990), and Brilliant Blue FCF (Flury et al., 1994). Coloring techniques have been used to map iodide, chloride, ammonium carbonate, or bromide (van Ommen et al., 1989; Wang et al., 2002).

There is no generally accepted approach to quantify the resulting dye patterns in the soil (Droogers et al., 1998). In earlier studies, dye patterns were copied onto transparent sheets and later digitized. Image

* Corresponding author. Tel.: +1-541-737-8719; fax: +1-541-737-4316.
E-mail address: markus@2hydros.de (M. Weiler).

0016-7061/$ - see front matter © 2003 Published by Elsevier B.V.
doi:10.1016/j.geoderma.2003.08.014

analysis has been used to extract the stained area from pictures obtained with a CCD camera (Hatano et al., 1992) or from photographed sections (Forrer et al., 2000). However, the spectral properties of a heterogeneous soil profile, dark humic substances, and soil structure in the picture are particularly difficult to filter and distinguish from dye by image analysis (Forrer et al., 2000).

Digital image analysis allows a quantitative description of dye patterns. Quantitative parameters can be subdivided into basic and morphometric parameters, like dye coverage or a geometric description of stained objects, and more complex parameters like the scaling properties and spatial statistics (Ogawa et al., 1999). They can be used to describe the pattern directly or they can be combined to classify the pattern (Kulli et al., 2003). Another possibility to subdivide quantitative parameters is to describe the dye pattern as a whole or to describe stained objects (Droogers et al., 1998). An example for describing the pattern as a whole is the dye coverage profile in a soil (Flury et al., 1994; Ghodrati and Jury, 1990; Perillo et al., 1999). Other examples of specific applications are the shape of individual pores (voids or cracks) defined by the ratio between area and perimeter (Bouma et al., 1977). Perillo et al. (1999) used dye patterns to calculate the total number of separate objects per depth to describe the preferential behavior of the flow process. Besides the analysis of dye patterns, the quantitative description of the soil structure of resin impregnated soils has initiated new methods in image analysis (McBratney et al., 1992; Ringrose-Voase, 1990), some of which can also be transferred to dye pattern analysis.

A more abstract way to quantify patterns is the mass fractal dimension to describe the fractal properties of space-filling objects. Hatano and Booltink (1992) pioneered this approach for soils and showed that the mass fractal dimension varies considerably both among soils and with depth for a given soil. More recently, Hatano and Booltink (1998) used the fractal dimension of horizontal dye patterns to explain the amount of outflow due to preferential flow. However, other studies showed the limitation of applying fractals, as the mass fractal dimension depends more on the image resolution and the thresholding algorithm used to classify the dye pattern than on the characteristics of the dye pattern (Baveye et al., 1998).

Spatial statistics of dye pattern can be used to describe the distribution of pores. For example, the point to nearest neighbor distances distribution (Droogers et al., 1998) and the minimal area of 50% of the dye mass (Vanderborght et al., 2002) have been used to characterize the movement of water between macropores and the surrounding soil matrix in horizontal dye patterns. Spatial statistical parameters such as the variogram apparently do not describe dye patterns better than basic parameters like the number of stained objects, average area per object and object shape (Droogers et al., 1998).

In many infiltration studies in soils with macropores, observations have been interpreted as being the result of different flow processes (Bouma et al., 1982; Bouma and Wösten, 1979; Buttle and House, 1997; Ehlers, 1975; Flury et al., 1994; McIntosh et al., 1999; Weiler and Naef, 2003a). The observed flow processes have been primarily divided into flow processes occurring in the soil matrix only and processes in macropores interacting with their immediate vicinity. Flow in the soil matrix may be macroscopically homogeneous or heterogeneous at the observation scale. In the latter case, two types of preferential flow have been identified: fingering in heterogeneously wettable soils (Bauters et al., 1998; Ritsema and Dekker, 1993), fingering at textural boundaries, or funnel flow by air trapping ahead of the wetting front (Ju and Kung, 1997; Kung, 1993). Interactions between macropores and the matrix are controlled by water supply into macropores, flow conditions in the macropores, and by water transfer from macropores into the surrounding soil matrix (Beven and Germann, 1982; Buttle and House, 1997; Faeh et al., 1997). Water transfer from macropores into the surrounding soil matrix, referred to as lateral infiltration (Beven and Clarke, 1986) or just as interaction (Weiler and Naef, 2003a), is one of the sensitive and critical processes for describing water flow in macroporous soils (Faeh et al., 1997; Logsdon et al., 1996). In particular, the quantity and rate of water flow across the macropore–matrix boundary largely determines the impact of macropores on the overall infiltration process and mixing regime of solutes (Weiler and Naef, 2003a).

Although research in dye pattern analysis is abundant by now, there is still no adequate method available to interpret the dye patterns directly in terms of the flow processes. Therefore, the prime objective of this study is to develop a method to classify the flow regime on the basis of dye patterns in vertical soil sections. Depth profiles of basic parameters such as dye coverage or geometric descriptions of stained objects provide some first approximate information about the flow regime. However, their information content is insufficient to link the characteristics of dye patterns to the underlying flow processes. We postulate that parameters describing single stained objects can be used to derive flow type profiles in a soil. We first define different flow types based on the occurring flow processes during infiltration. Then we quantify the characteristics of dye patterns and derive the rules to classify the vertical dye patterns flow type profiles.

A second objective is to quantify interaction between macropores and the surrounding soil matrix on the basis of dye patterns in horizontal soil sections. These patterns provide detailed information about the location of macropores and the arrangement of stained matrix relative to macropores. We develop a method based on statistical parameters to evaluate the distances to the nearest conducting macropore on the basis of earlier studies (Droogers et al., 1998; Vanderborght et al., 2002).

2. Materials and methods

2.1. Study sites

At three field sites in Northern Switzerland (Rietholzbach, Heitersberg, and Niederweningen) we conducted sprinkling experiments with a Brilliant Blue solution at two irrigation rates, 60 mm h^{-1} (high) and 12 mm h^{-1} (low) with a total irrigation of 75 mm, and two different initial soil moisture conditions referred to as "dry" (no input within 4 weeks) and "wet" (75 mm rainfall at the previous day) (Weiler and Naef, 2003a). Under dry soil moisture conditions, the soil water suction was between 100 and 600 hPa; under wet conditions, the suction was between 30 and 80 hPa. The saturated hydraulic conductivity of the soil matrix of all sites is between 10 and 20 mm h^{-1} for the topsoil and between 2 and 5 mm h^{-1} (except for Niederweningen 40 mm h^{-1}) for the subsoil. All of the sites are grassland and their soils exhibit a macropore structure dominated by vertically oriented earthworm burrows (>2 mm diameter). However, other soil characteristics differ (Table 1). The sprinkling area was 1 × 1 m.

The flow pattern of the infiltrated water was visualized by adding 4 g l^{-1} of the food dye Brilliant Blue FCF (C.I. 42090) to the sprinkling water. This dye was chosen because it is a good compromise between visibility, mobility, and toxicity for visualizing flow pathways in the vadose zone (German-Heins and Flury, 2000). The properties of Brilliant Blue FCF have been studied in detail by Flury and Flühler (1995), German-Heins and Flury (2000), Ketelsen and Meyer-Windel (1999), and Perillo et al. (1998). The sorption isotherm of this substance is often highly non-linear (Ketelsen and Meyer-Windel, 1999; Perillo et al., 1998). When applied at a concentration of 4 g l^{-1}, Brilliant Blue FCF is still visible after considerable dilution and adsorption

Table 1
Soil properties of the experimental sites

Site	Soil classification[a]	Geological parent material	Average values for distinct soil horizons			
			Horizon	Depth (cm)	Density (g cm^{-3})	Soil texture
Rietholzbach	Mollic Cambisol	Conglomerates (molasse)	A	0–30	1.14	loam
			A/B	30–60	1.25	loam
			B	60–100	1.35	clay loam
Heitersberg	Umbric Cambisol	Moraine	A	0–20	1.34	loam
			A/B	20–45	1.57	loam
			B	45–100	1.66	loam
Nieder-weningen	Eutric Cambisol	Sandstone (molasse)	A	0–30	1.41	sandy clay loam
			B	30–55	1.44	sandy loam
			C	55–100	1.42	sandy loam

[a] FAO–UNESCO (1988).

over flow distances (German-Heins and Flury, 2000). Due to the non-linear sorption isotherm, Brilliant Blue FCF fronts are self-sharpened and produce a strong color contrast to the soil material (German-Heins and Flury, 2000; Kasteel et al., 2002).

2.2. Sampling scheme

One day after sprinkling, four or five parallel vertical soil sections of 100 by 100 cm were prepared, starting 15 cm from the downslope border at each plot. The spacing of the vertical sections was 5–7 cm. The following day, four or five horizontal soil sections were prepared between 5 and 70 cm depth parallel to the soil surface with a closer spacing near the soil surface. The horizontal sections were directly adjacent to the last vertical section and covered an area of 100 × 50 cm. The sections were carefully prepared with a spatula and loose particles were removed with a vacuum cleaner (Weiler and Naef, 2003a). Thus, the earthworm burrow openings became clearly visible allowing the determination of the macropore locations.

The soil sections were photographed according to Forrer et al. (1999). The soil profiles were photographed under daylight conditions beneath a whitish opaque foil (light tent) to diffuse the light and avoid direct radiation. White reflection panels were mounted on three sides of the soil sections to balance and compensate differences in illumination. A gray frame with a ruler and a Kodak gray and color scale was attached to the frame. A standard color slide film (Kodak Ektachrome Elite 200) was used without any optical filters.

In addition to the soil sections, we prepared calibration patches of 5 × 5 cm by applying Brilliant Blue solutions of 0, 400, 800, 1600, 3200, and 4000 g l^{-1} onto horizontal soil sections in the topsoil and in the subsoil adjacent to the vertical sections. These calibration solutions were applied onto the soil until saturation and then the patches were photographed. The patches were later used in the image analysis procedure to detect the visibility limit and to classify the stained areas into concentration categories.

2.3. Image processing and classification

We applied rigorous, repeatable methods of image processing to classify the dye patterns (Fig. 1) using the software package IDL (Research Systems). The picture for each soil section was digitally scanned with a resolution of 3072 × 2048 pixels. Geometric distortion of the pictures was corrected by establishing a relationship between the location of pixels in the image and the corresponding coordinates on the soil profile (Richards, 1986). An algorithm defining the spatial transformation and an algorithm for gray-level interpolation are required. We selected “tie points” (TPs) from the ruler at the gray frame. TPs are a subset of pixels whose locations are known in the distorted and corrected image. Then, knowing the location in the distorted image and on the soil profile of a subset of pixels, a first-order polynomial was fitted with a least-square estimation to the TPs. Because TPs were only selected near the border of the image, a first-order polynomial minimizes the geometric error in the image further away from TPs (Richards, 1986). The geometric error was calculated to be at most two pixels (2 mm on the soil section). We chose nearest neighbor resampling for the gray-level interpolation because corrected images still consists of the original brightness values, simply rearranged in position to give correct image geometry (Richards, 1986). After geometric correction, one pixel corresponds to a square of 1 × 1 mm on the vertical section and 0.5 × 0.5 mm on the horizontal section.

Since the soil profiles were only illuminated with diffuse daylight, the lower part of the vertical sections and the corners of the horizontal sections were darker than the other portions of the image. These differences were compensated using background subtraction. The RGB (red–green–blue) image was converted into HSV (Hue–Saturation–Value) color space. The background image, which shows the variation of illumination in the Value-space (V-space), was interpolated from 15 to 20 actual values of the gray frame to a smooth quintic surface and divided by the mean of the V-space. The corrected V-plane, being the product of the background image and the original V-space image, together with the unchanged H- and S-plane was finally converted back into the RGB color system.

Because the spectral composition of daylight changes during the day and the photographs were taken at different times of day, the brightness value of every color channel differs among the images. A color adjustment was applied to warrant comparability of

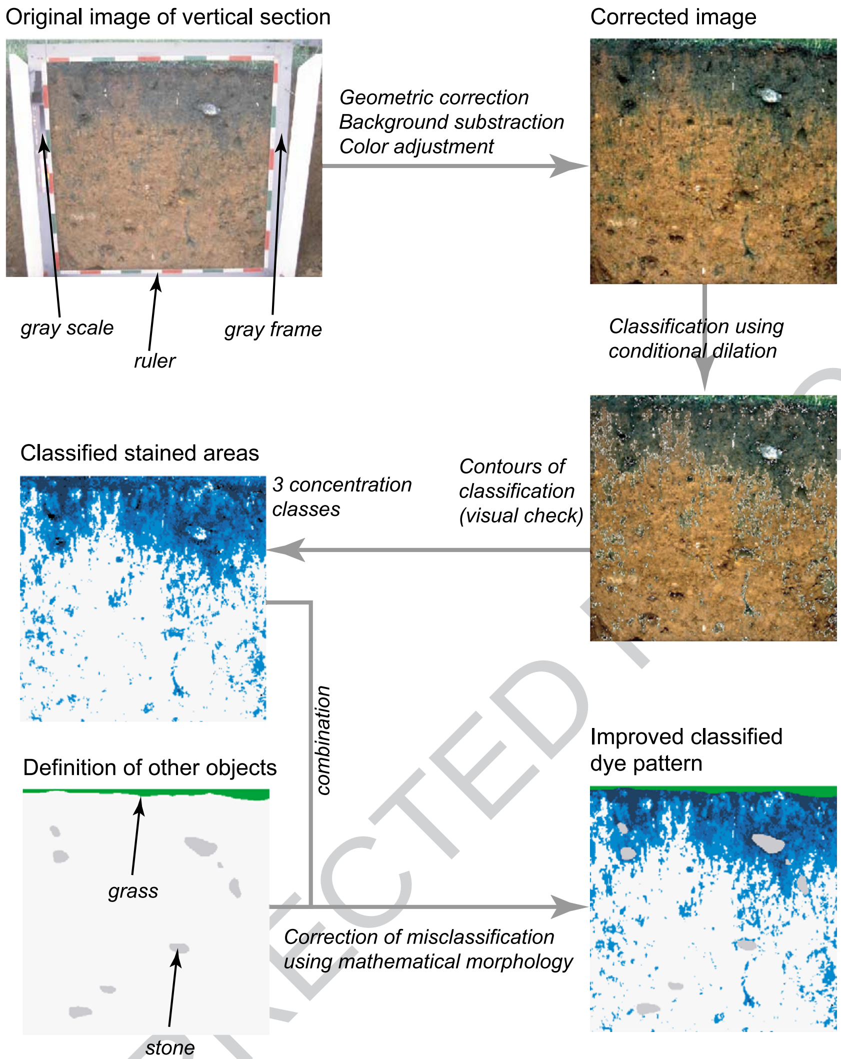

Fig. 1. Flow chart of the image analysis procedure for an image of a vertical soil section.

the images. The Kodak gray scale, which consists of 20 patches from white to black, was used for this adjustment. The mean brightness value of every channel for the patch no. 6 of the gray scale was set to 255, because very bright regions were not of interest for the analysis. The darkest patch was set to 0 and the remaining values were linearly stretched between 0 and 255 to calculate normalized values for every channel. Thus, resulting in an objective brightness and contrast enhancement. Finally, the images were cropped along the gray frame resulting in a size of approximately 1000×1000 pixels for the vertical sections and 2000×1000 pixels for the horizontal sections. In Fig. 1, the combined effects of geometric correction, background subtraction, and color adjustment are documented.

The heterogeneous spectral background resulting from the heterogeneous soil profiles corrupts the estimation of the spatial distribution of tracer concentration on the images (Forrer et al., 2000). Similar to the work of Aeby et al. (1997), we developed and applied a robust semi-supervised classification technique to discriminate stained from unstained areas and to classify the tracer concentration into three categories. Image segmentation, where each pixel is assigned to a particular object or region, was chosen as classification technique (Castleman, 1996). The thresholding of the gray level histogram yields the best results if the objects (stained areas) and the background (unstained soil) are characterized with a bimodal histogram. In cases like this, the threshold value can be chosen at the minimum that separated the two maxima of the histogram (Castleman, 1996). Using the calibration patches with their different dye concentrations, the spectral properties of stained and unstained areas were evaluated. In HSV-color space, the closest relation between the H and V values and dye concentration was detected using scatter plots between various color parameters and the logarithm of dye concentration (Ewing and Horton, 1999). However, the values were not linearly correlated to the dye concentration and soil heterogeneity diminishes the correlation. Therefore, instead of adapting a linear regression model to classify the images (Forrer, 1997), we developed an algorithm that separates different concentrations and unstained areas independently from the underlying structure and color of the soil. A variable T was calculated as:

$$T = \frac{H}{360\pi}(1 - V) \tag{1}$$

where H values are given in grad and V values range between 0 and 1. T was then used in combination with the concentration patches to classify the images into four categories: (i) "unstained areas" ($c < 0.4$ g l^{-1}) = detection limit with this method, (ii) "low concentration" (0.4 g $l^{-1} < c < 1.0$ g l^{-1}), (iii) "medium concentration" (1.0 g $l^{-1} < c < 3.0$ g l^{-1}), and (iv) "high concentration" ($c > 3.0$ g l^{-1}).

A conditional dilation algorithm (Serra, 1988) was used to improve the classification results. This algorithm uses two thresholds to partition the image into three classes. The upper and lower classes positively belong to the object or background. The central class is the uncertainty range. A pixel value belonging to the uncertainty range is attributed to the upper or lower class depending on the values of the neighboring pixels (contextual classification). The algorithm works iteratively until no more uncertain pixels can be found in the neighborhood of already classified pixels. Finally, the conditional dilation algorithm results in images with a higher spatial coherence and a lower interference of noise.

This process provided a classification of areas as either unstained or stained. Stained areas were then further classified into three concentration categories with thresholds defined according to the calibration patches at each experimental site. Because of slight variations in the optimal threshold for the classification, an initial guess was used to classify the image. After a visual check, the result of the initial guess was not satisfying for 15% of all images. These images were reclassified with a variation of the threshold (Fig. 1). Finally, a median filter with a rectangular area of interest of three pixels was applied to remove misclassified single stained pixels.

In addition to the stained areas, macropores (holes or cracks with an area larger than 2 mm^2) that were visible on the images of the horizontal sections were classified. Since macropores appeared as darker areas surrounded by stained or unstained areas, they had to be detected independently from the surrounding reflectivity. Visible macropores were manually digitized for subsets of five horizontal sections and different classification algorithms were then tested against the subsets. To be acceptable, a classification algorithm must detect only macropores, correctly classify shape and size of macropores, and be independent of other image properties like illumination, surface roughness, and dye coverage. We calculate a variable r for each pixel (i,j) of the grey color image (V-space), which was then used to perform an image segmentation with the conditional dilation algorithm;

$$r(i,j) = \frac{w^2 V(i,j)}{\sum_{m=0}^{w-1}\sum_{n=0}^{w-1} V(i+m-0.5w, j+n-0.5w)} \tag{2}$$

where w is the window width of the mean filter (set to 40 in order to represent the scale of the observed macropore openings) and V is the value of the V-color space. Thus, r quantifies the deviation of the V value from the average within the defined window. We determined an average threshold of 38 ± 9 (V ranges from 0 to 100) for all horizontal images.

On average, the correctly classified macropore area for all training sets was 67% of the digitized macropore area. The percentage of correctly classified individual macropores was 90%. After the segmentation procedure, a median filter with a dimension of 4×4 pixels was applied to remove classified areas with an area smaller than or equal to 1 mm^2 (2×2 pixels).

Grass at the soil surface, large stones, and shadows near the border of the image were manually identified as well in order to enhance the image truth of the analysis (Fig. 1). The upper border, identified with the soil surface, was manually delineated and the area above was classified as grass. For all vertical images, the average soil surface was defined as the lowest row of the image, in which the classified grass coverage exceeded 50% of the total image width. This row is the reference to calculate soil depth within the vertical image. Large stones (diameter >20 mm) were manually delineated, because of their distinctly different reflectance. The digitized stones mark areas with no-flow inside and occasionally pronounced flow outside close to the stone surface. The horizontal sections show also shadows near the edge of the image, where soil was accidentally removed during excavation. Such areas were manually delineated and were not considered in the further analysis of the images.

After applying the classification procedures, the classified dye patterns still showed some flaws, such as small areas in the humic topsoil classified as dark areas but being stained in reality, and small connected stained areas classified as being unconnected (Fig. 1). To correct these misclassifications, tools from mathematical morphology was applied in addition to the image analysis (Soille, 1999). Mathematical morphology uses set theory, geometry, and topology to analyze the geometric structure of an image by probing it with a structuring element (operator) characterized by shape, size, and location of its center. Such operators allow distinguishing meaningful information from irrelevant distortions. We used two types of mathematical morphology operations, namely dilation and erosion. Dilation, in general, causes objects to grow in size and erosion causes them to shrink. The extent and way of growing and shrinking depends on the shape and size of the structuring element. We selected appropriate structuring elements for the horizontal and vertical sections (Weiler, 2001). One algorithm was developed to find small black holes in stained areas; the second eliminated small unstained areas within larger stained areas. The combination of the two algorithms resulted in a significant improvement of the classification for all sites (Weiler, 2001).

2.4. Conventional analysis of vertical dye patterns

We applied stereological methods to derive variation of basic morphometric parameters with depth. Stereological methods relate parameters describing three-dimensional structures to measured two-dimensional parameters (Weibel, 1979). Structural parameters can be correctly estimated if the structure is isotropic or if a random sampling method is used for an anisotropic structure. The horizontal dye patterns showed that the dye patterns are isotropic for each depth. From a variety of possible stereological parameters, we selected two parameters describing the density of stained structures in space: (1) the volume density V_V, which corresponds to dye coverage as measured in similar dye pattern related studies, and (2) the surface area density S_V.

The volume density can be estimated from one or two-dimensional information, because the length density L_L, areal density A_A, volume density V_V, and fraction of pixels, which are stained P_P, are equal (Weibel, 1979):

$$V_V = A_A = L_L = P_P \qquad (3)$$

The volume density can be determined from the fraction of pixels laying in the structure. Thus, the volume density profile is estimated from the fraction of stained pixel per depth. The surface area density S_V defined in three dimensions is the surface area of a structure divided by the volume of the reference space. It can be estimated from the perimeter density B_A defined in two dimensions or the intercept density I_L defined in one dimension. The intercept density can be determined from the number of intercepts of a transect line with the structure divided by the total length of the line. The relation is given by (Weibel, 1979):

$$S_V = 4B_a/\pi = 2I_L \qquad (4)$$

Hence, the surface area density profile is estimated from the intercept density calculating the number of intercepts between unstained and stained pixels per depth. The volume density profile and the surface density profile were calculated at a vertical resolution of 1 mm for all four to five vertical dye patterns per experiment. Starting at the soil surface ($z = 0$), the volume and surface density profile was calculated and the section-specific profile was averaged for each experiment. The standard deviation was also calculated, but it was not used for further analysis, because the variation was usually low. The volume density profiles and surface area density profile were calculated for the stained areas without differentiating among the concentration classes, because in this paper, we were mainly interested in the stained objects as a whole.

2.5. Flow process oriented analysis of vertical dye patterns

For the following analysis, we categorize five different flow types using stained path width (SPW) profiles (Table 2). Three of them are related to macropores and two of them involving the soil matrix only. The dye pattern is a realization of the underlying flow processes given the amount of infiltrated solution traced with a mobile dye of given sorption characteristics. Since the last factor is kept constant for all of our experiments, flow processes explain the differences between the dye patterns.

An obvious way to categorize characteristic dye patterns is by the extent and distribution of stained objects. For example, long narrow stain shapes dominate the characteristic dye pattern of macropore flow with low interaction, whereas macropore flow with mixed interaction shows a broader distribution of shapes. Therefore, a distribution of widths of stained objects at each depth is one option to categorize stained patterns.

One way to calculate the width of stained three-dimensional objects at a given soil depth is to measure their one-dimensional extension within two-dimensional dye patterns. In stereology, this one-dimensional extension is called the intercept length. It estimates the cross-sectional object area provided the object is isotropic (Weibel, 1979). Therefore, the object width at a given depth in a vertical dye pattern may be used as a proxy for the size of the object at this depth. Because the object width describes the extension of a stained flow pathway, it is referred to as SPW. The SPW profile for each object can be calculated for each vertical dye pattern, which results in a frequency distribution of SPWs for each soil depth. The SPW was calculated without differentiating between the concentration classes of the stained areas. The SPW

Table 2
Definition of flow types in soils that can be distinguished by dye pattern

Flow type	Soil characteristics	Characteristic dye pattern	Proportion of SPW for <20 mm	Proportion of SPW for >200 mm
Macropore flow with low interaction	Macropores in a low permeable or saturated soil matrix		>50%	>20%
Macropore flow with mixed interaction (high and low)	Macropores in a heterogeneous soil matrix or macropores with variable macropore flow		20-50%	<20%
Macropore flow with high interaction	Macropores in a permeable soil matrix (texture or aggregation)		<20%	<30%
Heterogeneous matrix flow and fingering	Spatially heterogeneous soil properties, e.g. wettability or flow instability		<20%	<30-60%
Homogeneous matrix flow	Permeable soils (texture or aggregation)		<20%	<60%

was then classified into three classes (< 20 mm, 20–200 mm, >200 mm) and the volume density of all objects within each class was calculated (Weiler and Naef, 2003a). The SPW classes were then sorted according to their size and the volume densities of the corresponding SPW class were stacked. Because the SPW classes are expressed on the basis of volume density, the maximum value corresponds with the volume density of all concentration classes. The SPW profile per experiment is derived by combining all vertical dye patterns of each experiment.

We distinguish five flow types based on the three categories of SPWs (Weiler, 2001). The chosen SPW limits of 20 and 200 mm are specific for our experiments. For example, the category < 20 mm represents flow pathways where the dyed solution flows primarily in macropores with only minor penetration of the surrounding matrix. We found that the volume density is not needed to distinguish the five flow types. Thus, the relative proportion of the three SPW classes was used to develop a classification rule. We tested this rule on differently structured dye patterns (Weiler, 2001). The classification rules are shown in the last two columns of Table 2.

The final flow type classification was performed by the following steps: (1) the three SPW categories at every soil depth were derived from the SPW profile and the respective proportions were determined; (2) they were classified according to Table 2; and (3) a median filter with a window width of 2 cm was applied to the resulting flow type profile to remove small-scale artifacts.

2.6. Analysis of horizontal dye patterns

The classified macropores in combination with the dye pattern of the horizontal sections are used to quantify the interaction between macropores and the surrounding soil matrix by characterizing the spatial distribution of stained areas relative to the macropores. First, the Euclidean distance from each pixel to the nearest macropore was computed from the classified horizontal sections and its frequency distribution was compiled. Then, we compiled the Euclidean distance only for stained pixels and then derived the corresponding frequency distribution. To analyze the staining relative to the total area around the macropores, we calculated the ration between the two derived frequency distributions. The resulting function is referred to as staining ratio. The staining ratio specifies the following characteristics of each horizontal dye pattern: the value at a distance of 1 mm indicates the proportion of stained macropores and the shape of the curve is a measure of the average staining distance and thus describes the pattern of the stained area in relation to the macropores.

3. Results and discussion

3.1. Conventional analysis of vertical dye patterns

The volume density profile gives a first overview of the dye patterns of the experiments. The volume density profile showed not only marked differences between the experimental sites, but also similarities depending on the treatment (Fig. 2). The profiles also include the classified SPW profiles, which are described in the next section.

Rietholzbach site: The volume density profiles show that the dye tracer stained mainly depths of 0–70 cm for the high irrigation rate. The same holds for the low rate, but only under dry initial moisture conditions. Under the low irrigation rate at wet initial moisture conditions, only the upper part of the profile was stained.

Heitersberg site: A pronounced staining of the upper soil layer was observed for all experiments. The initial soil moisture conditions determined the thickness of the stained upper soil layer, especially for the high irrigation rate. Below 30 cm, the staining was weak but continuous. The volume density of the subsoil was higher at dry initial moisture conditions, but the differences due to different irrigation rates were minor.

Niederweningen site: The profiles differed distinctly from the results of the other sites. Under the low irrigation rate, the staining of the top soil was almost complete. The horizon 30–40 cm was definitely less intensely stained, which suggests significant by-passing, because the staining increased again below 40 cm. Depth and maximum of volume density depended on the treatment. The staining did not reach the bottom of the vertical soil section.

Overall, the volume density profiles under the low irrigation rate at the dry initial moisture conditions

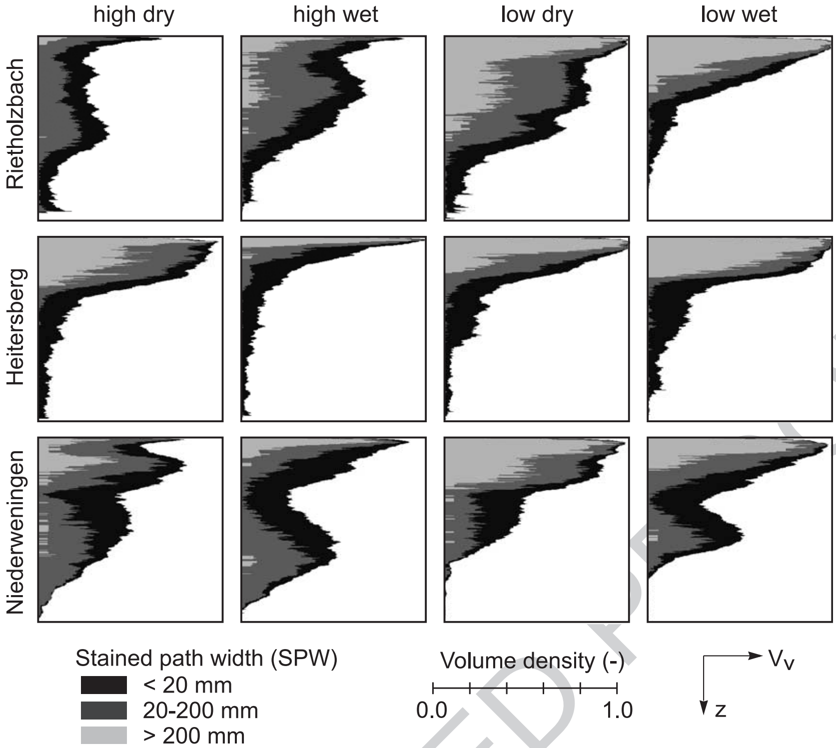

Fig. 2. Volume density profiles of vertical dye patterns ($z = 0-100$ cm) based on averaging four to five sections per experiment. The profiles are subdivided into three SPW classes (< 20 mm, 20 – 200 mm, >200 mm). The four experimental treatments were irrigation rate (high and low) and initial soil water content (dry and wet).

were more similar among sites compared to the other treatments. In addition to the volume density profile the surface area density profiles are shown in Fig. 3.

Rietholzbach site: Under the high irrigation rate, the surface area density changed little with depth; the geometry of the stained areas was similar at the two initial moisture conditions. The pattern for the experiments with the low irrigation rate showed a distinct peak at 60 cm depth (dry) or at 25 cm depth (wet). These peaks coincided with a sharp decrease of the volume density, where the contiguous dye pattern separated into many smaller stained objects. This phenomenon was also observed at the other sites.

Heitersberg site: The four surface area density profiles were quite similar to each other. The surface density was relatively large compared to the volume density. Only small stained objects with large surface areas can explain this behavior. Especially patterns resulting from the low irrigation rate showed a large surface area density in the middle part of the profile.

Niederweningen site: All profiles showed a distinct peak in the depth range of 30 – 40 cm. This range correlates to local minima in the volume density. The pattern disintegrated into a lot of small stained objects with a low volume but high surface area density in this particular depth range. The surface area density declined below 40 cm despite an increase of the volume density. Here, the pattern changed to larger stained objects with a relatively low surface area density.

The surface area density profiles should be interpreted together with the volume density profiles, since the volume density can be different for the same surface area density. For example, the surface area density and the volume density are both low when small stained areas have also a small surface. However, the volume density can be high when the surface area density is low, if a stained object covering the whole soil volume has a small surface. However, even the combination of volume density and surface area

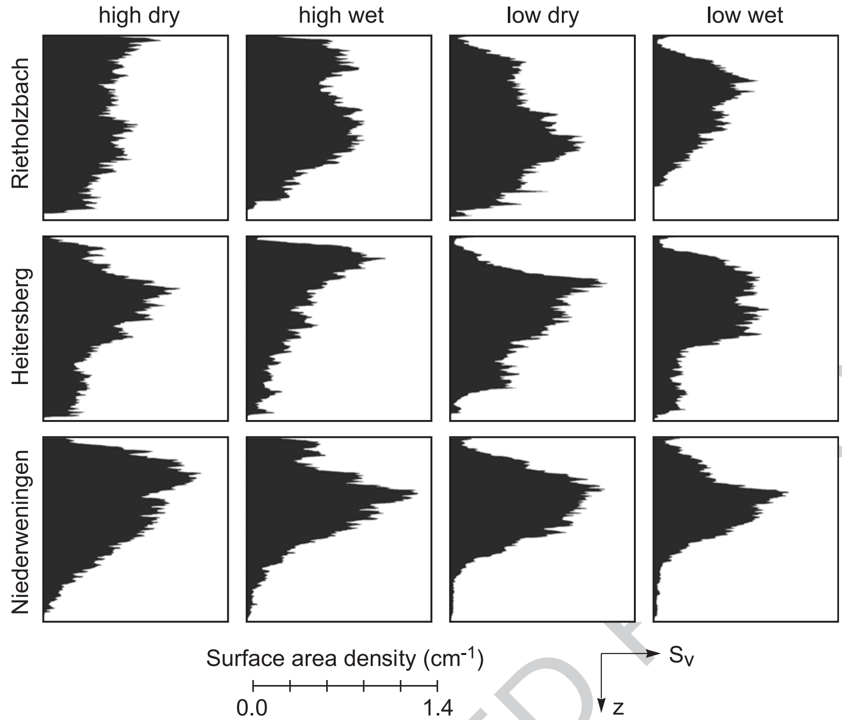

Fig. 3. Surface area density profiles of vertical dye patterns ($z = 0-100$ cm). The four experimental treatments were irrigation rate (high and low) and initial soil water content (dry and wet).

density is not a sufficient indicator to analyze the flow types that resulted to the observed dye patterns.

3.2. Flow types of vertical dye patterns

Using the SPW profiles (see in Fig. 2) and the classification rules in Table 2, the classified profiles of flow types for each experiment were calculated (Fig. 4). The flow type profiles illustrate the continuity of each flow type and a frequently occurring transition from a specific flow type to another one, but also differences and similarities for the experiments.

Rietholzbach site: The classified flow types under high and low irrigation rate differed considerably. Under the high irrigation rate, we observed mainly macropore flow with a high interaction in the upper 60 cm, without a transition zone at the soil surface. Under the low irrigation rate, there were transitions from homogeneous matrix flow near the soil surface to heterogeneous matrix flow and then to macropore flow with interaction progressing from high to low with depth. The vertical range of influence of a given flow type depended on the initial soil moisture conditions. For example, macropore flow with low interaction dominated the flow below 60 cm for all experiments.

Heitersberg site: The flow type profiles were similar for all experiments (Fig. 4). In the upper soil layer, matrix flow dominated. The depth of matrix flow was higher under dry initial soil moisture conditions. Below 30 cm, there was a sharp transition towards macropore flow with low interaction in all experiments. Thus, the experimental treatments did not influence the flow types in the subsoil (>30 cm depth).

Niederweningen site: Macropore flow with high interaction dominated at depths >50 cm (Fig. 4). The maximum depth of this zone depended on the experimental treatment. In the depth range of 30–50 cm, macropore flow with mixed or low interaction was detected for all experiments. In the top soil layer under dry initial conditions, matrix flow types are more pronounced. At this site, the upper soil layer channels the water into macropores, the water bypasses the next layer by macropore flow with low interaction, and

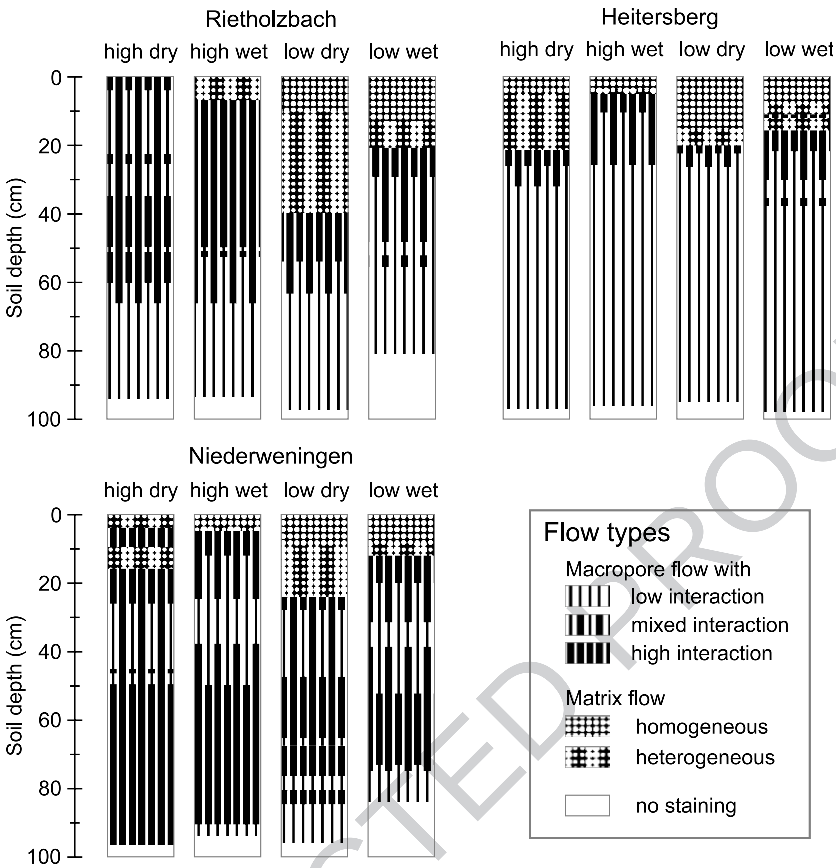

Fig. 4. Flow type profiles classified from the vertical dye patterns using a classification rule (Table 2) applied to the stained path width profiles. The four experimental treatments were irrigation rate (high and low) and initial soil water content (dry and wet).

macropores interacted with the soil matrix in the deepest layer.

3.3. Horizontal dye patterns

Instead of presenting all results of the horizontal dye pattern analysis, we selected six examples representing the range of characteristic pattern in the data. For each horizontal section, the frequency distributions of the distance to the nearest macropore for all pixels and only stained pixels together with the staining ratio (Fig. 6) is compared with the classified dye pattern (Fig. 5).

The horizontal dye pattern (Fig. 5a) at the Rietholzbach site under high irrigation rate, at dry initial moisture conditions and at depth ($z = 39$ cm) contained small contiguously stained areas, mainly grouped around macropores. There were also large unstained areas. For this horizontal section, the frequency distributions for all pixels and unstained pixels are broad and the frequencies for larger distances are still high (Fig. 6a). Thus, the extent of stained areas around macropores is quite large, which can also be seen in the gradual slope of the staining ratio. The staining ratio starts at a value of around 0.8, because the immediate surrounding of some macropores was not stained.

The pattern at a depth of 10 cm at the Rietholzbach site under low irrigation rate and at dry initial moisture conditions (Fig. 5b) was quite contiguous with only few macropores. However, there were also unstained areas. Both frequency distributions have a similar shape and show a distinct broad peak and a gentle recession (Fig. 6b). The staining ratio starts at

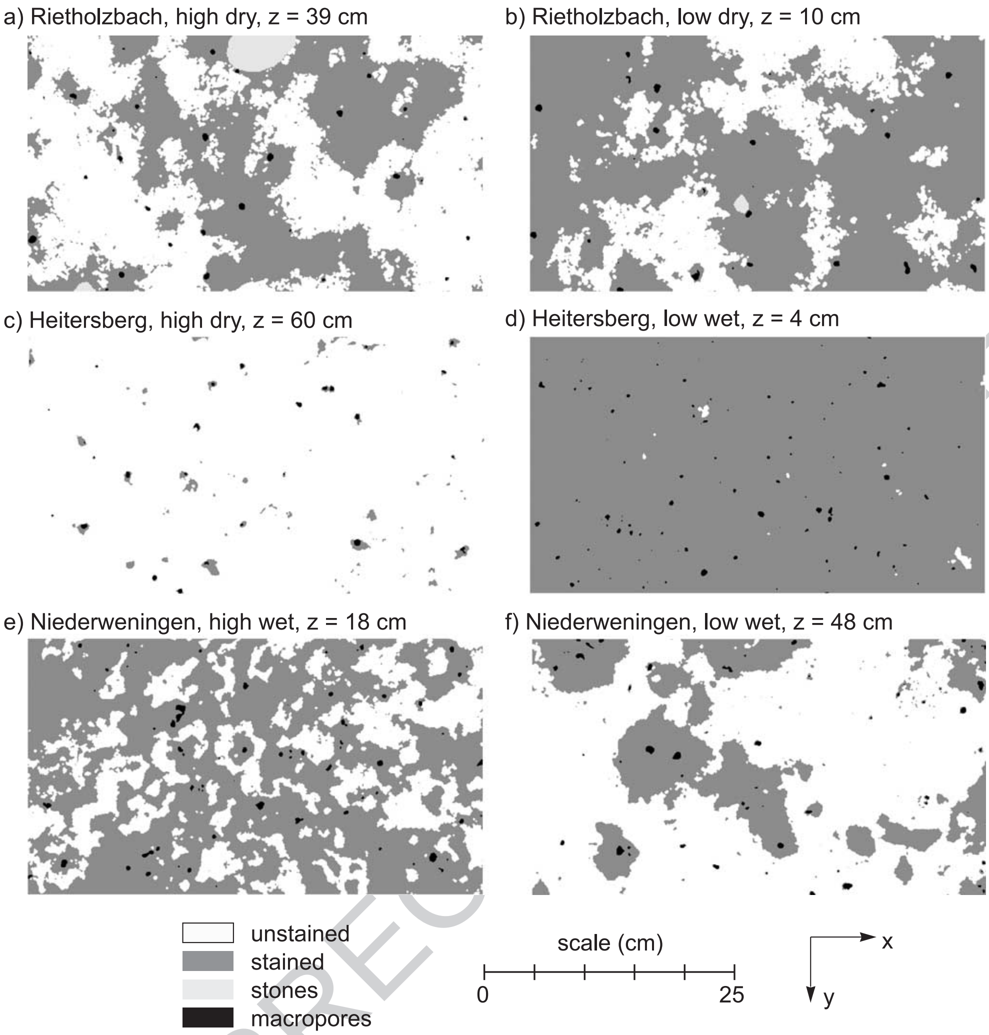

Fig. 5. Selected examples of horizontal dye patterns showing unstained and stained soil matrix together with classified macropores (>1 mm^2). The four experimental treatments were irrigation rate (high and low) and initial soil water content (dry and wet). The depth (z) of each horizontal section is the average depth of the profile measured from the soil surface.

1.0, indicating that all macropores were surrounded by stained matrix, and levels off at around 0.75 at a distance of 20 mm to the nearest macropore. The high staining ratio is a result of the high interaction between the macropores and the permeable soil matrix.

At the Heitersberg site under high irrigation rate and dry moisture conditions, the section at a depth of 60 cm shows only small stained areas around the macropores (Fig. 5c). The corresponding frequency distribution of stained pixels is characterized by a very steep decline for a short distance (Fig. 6c). The frequency distribution for all pixels is similar to toe distributions at the Rietholzbach site. Hence, the staining ratio shows also a steep decline and indicates that around 60% of the macropores were stained. It is difficult to observe the small-scale staining around the macropores on the vertical sections, indicating that the preparation of horizontal section may be necessary for detecting macropore flow combined with low interaction between the macropores and the surrounding soil matrix.

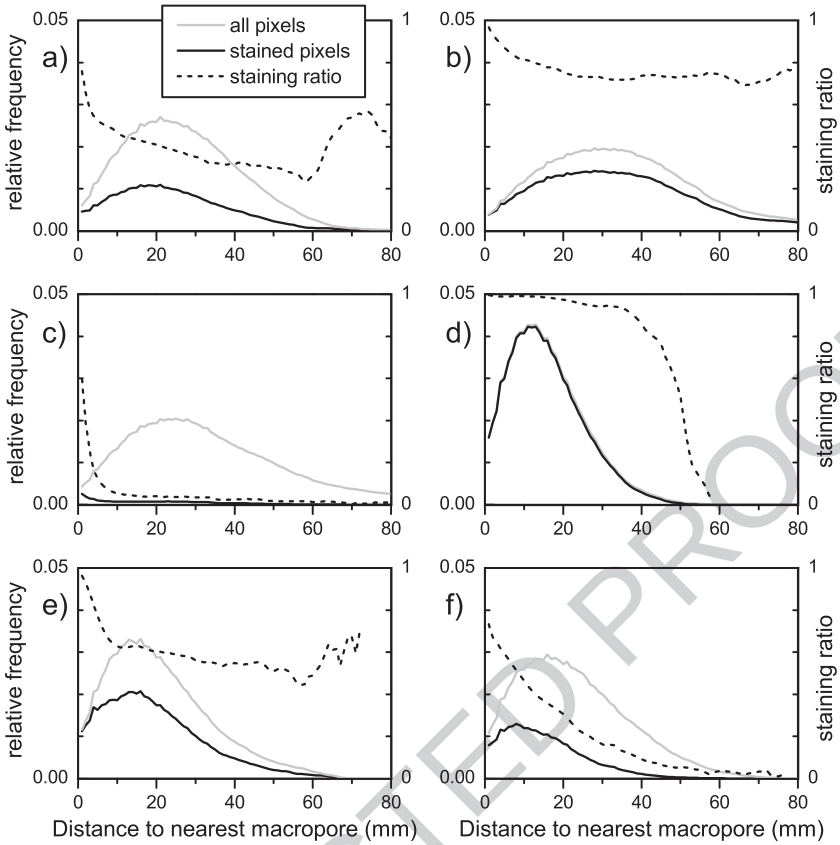

Fig. 6. Frequency distributions of the distance to the nearest macropore for all pixels and only stained pixels together with the staining ratio of selected horizontal dye patterns. The distributions match up to Fig. 5 with (a) Rietholzbach, high dry, $z=39$ cm, (b) Rietholzbach, low dry, $z=10$ cm, (c) Heitersberg, high dry, $z=60$ cm, (d) Heitersberg, low wet, $z=4$ cm, (e) Niederweningen, high wet, $z=18$ cm, and (f) Niederweningen, low wet, $z=48$ cm. The four experimental treatments were irrigation rate (high and low) and initial soil water content (dry and wet).

At the Heitersberg site under low irrigation rate and at wet initial moisture conditions, the dye pattern near the soil surface ($z=4$ cm) showed a large stained area and only some small unstained spots (Fig. 5d). Because the macropore density was quite high and most of the area was stained, the frequency distributions result in a distinct peak at a distance of 13 mm (Fig. 6d). The corresponding staining ratio shows a nearly constant value of 1.0 to a distance of 40 mm, then dropping down to zero.

The dye pattern at a depth of 18 cm at the Niederweningen site under high irrigation rate and at wet initial moisture conditions was quite different than the patterns already discussed (Fig. 5e). The pattern showed some kind of a stained network. Both frequency distributions show a long tailed shape (Fig. 6e). The staining ratio drops at low distance (<10 mm) and then levels off at a value of 0.6. The asymptotic shape of the staining ratio is a result of the networked dye pattern. The staining around the macropores stops only in some directions, but in other directions, the staining expands. This networked pattern may be a result of a heterogeneous soil matrix due to cracking and aggregation.

The last example is the dye pattern in the subsoil ($z=48$ cm) for the experiment at the Niederweningen site under low irrigation rate and at wet initial moisture conditions (Fig. 5f). This pattern is characterized by some larger stained areas around some of the macropores. Compared to the other examples, the stained areas were well-defined. The frequency distribution for all pixels shows a relative broad peak at a distance of 16 mm. The corresponding distribution for stained pixels is highly skewed and peaks at a distance of 8 mm. The staining ratio is characterized by a slow, gradual decrease. The slow decrease is a result of the large, well-defined stained area around the macropores. The value of 0.73 at 1 mm distance indicates that in 25% of the macropores water did not flow to stain the surrounding soil matrix. The unequal distribution of flow in macropores can be explained by the initiation process of macropore flow (Weiler and Naef, 2003b).

4. Conclusions

We further developed the processing and classification of dye patterns form vertical and horizontal soil sections based on earlier studies (Aeby et al., 1997; Forrer et al., 2000). The fast and objective method allows clear delineation of stained and unstained areas and classification of stained areas into concentration categories. Macropores were correctly classified with a low error.

The conventional analysis of dye pattern deriving the volume density (dye coverage) profile and the surface density profile from several dye patterns allows recognizing various infiltration mechanisms in natural soils. However, this analysis needs interpretation and cannot be directly used to distinguish different flow processes. Therefore, we propose a classification which a priori identifies five flow types (macropore flow with low, mixed, and high interaction and heterogeneous and homogeneous matrix flow). This flow type definition is based on the assumption that all observed heterogeneities are due to macropore flow and heterogeneous matrix flow, hence other structural properties (e.g., impeding layers, layer boundaries, water repellency) might produce additional patterns that are not yet included in the classification. Although the classification only determines the flow types for each depth increment without considering the overall dye pattern, the results showed a logical sequence of flow types in the soil profile. These flow type profiles can serve as definitions of infiltration properties or even as a hydrological soil classification in general. Applying the flow type classification to dye patterns derived form infiltration into soils with different properties; a database can be developed where soil properties or landscape elements specifying preferential flow can be extracted.

The method of analyzing horizontal dye patterns quantifies the spatial relationship between visible macropores and stained soil matrix. The resulting frequency distributions of the distance to the nearest macropore for all pixels and only stained pixels together with the staining ratio capture this relation. The distributions characterize not only the dye pattern around macropores, but can be used to explore and compare the interaction between macropores and soil matrix in more detail.

The separate analysis of vertical and horizontal dye patterns showed that flow types in soils during infiltration can be described by different approaches. Vertical dye patterns reveal a sequence of different flow types within the soil profile. Horizontal dye patterns illustrate the detailed link between flow in the macropores and the interaction with the surrounding soil matrix. Combining both techniques support and extend each other. The decision of whether to apply both or one single technique depends mainly on the objective of the study. However, using dye patterns directly as information of flow types in the soils is a step forward from using dye patterns simply as nice qualitative pictures that illustrate preferential flow in soils.

Acknowledgements

This work was funded by the Swiss Federal Institute of Technology in Zürich within the project 'Investigation of the water exchange mechanisms between preferential flow paths and the soil matrix'. We would especially like to thank Felix Naef for his support during this study and Thomy Keller for his help during the field experiments. Finally, we would like to thank Richard Keim for considerably improving the manuscript.

References

Aeby, P., Forrer, I., Steinmeier, C., Flühler, H., 1997. Image analysis for determination of dye tracer concentrations in sand columns. Soil Sci. Soc. Am. J. 61, 33–35.

Bauters, T.W.J., DiCarlo, D.A., Steenhuis, T.S., Parlange, J.-Y., 1998. Preferential flow in water-repellent sands. Soil Sci. Soc. Am. J. 62, 1185–1190.

Baveye, P., Boast, C.H., Ogawa, S., Parlange, J.Y., Steenhuis, T., 1998. Influence of image resolution and thresholding on the apparent mass fractal characteristics of preferential flow patterns in field soils. Water Resour. Res. 34 (11), 2783–2796.

Beven, K.J., Clarke, R.T., 1986. On the variation of infiltration into a homogeneous soil matrix containing a population of macropores. Water Resour. Res. 22 (3), 383–388.

Beven, K., Germann, P., 1982. Macropores and water flow in soils. Water Resour. Res. 18 (5), 1311–1325.

Bouma, J., Wösten, J.H.M., 1979. Flow patterns during extended saturated low in two, undisturbed swelling clay soils with different macrostructures. Soil Sci. Soc. Am. J. 43, 16–22.

Bouma, J., Jongerius, A., Boersma, O., Jager, A., Schoonderbeek, D., 1977. The function of different types of macropores during saturated flow through four swelling soil horizons. Soil Sci. Soc. Am. J. 41, 945–950.

Bouma, J., Belmans, C.F.M., Dekker, L.W., 1982. Water infiltration and redistribution in a silt loam subsoil with vertical worm channels. Soil Sci. Soc. Am. J. 46, 917–921.

Buttle, J.M., House, D.A., 1997. Spatial variability of saturated hydraulic conductivity in shallow macroporous soils in a forested basin. J. Hydrol. 203, 127–142.

Castleman, K.R., 1996. Digital Image. Processing Englewood Cliffs, New York. 667 pp.

Droogers, P., Stein, A., Bouma, J., de Boer, G., 1998. Parameters for describing soil macroporosity derived from staining patterns. Geoderma 83, 293–308.

Ehlers, W., 1975. Observation on earthworm channels and infiltration on tilled and untilled loess soil. Soil Sci. 119 (3), 242–249.

Ewing, R.P., Horton, R., 1999. Discriminating dyes in soil with color image analysis. Soil Sci. Soc. Am. J. 63, 18–24.

Faeh, A.O., Scherrer, S., Naef, F., 1997. A combined field and numerical approach to investigate flow processes in natural macroporous soils under extreme precipitation. Hydrol. Earth Syst. Sci. 1 (4), 787–800.

Flury, M., Flühler, H., 1995. Tracer characteristics of brilliant blue FCF. Soil Sci. Soc. Am. J. 59, 22–27.

Flury, M., Flühler, H., Jury, W.A., Leuenberger, J., 1994. Susceptibility of soils to preferential flow of water: a field study. Water Resour. Res. 30 (7), 1945–1954.

Forrer, I., 1997. Solute Transport in a Unsaturated Field Soil: Visualization and Quantification of Flow Patterns Using Image Analysis, Zürich. 128 pp.

Forrer, I., Kasteel, R., Flury, M., Flühler, H., 1999. Longitudinal and lateral dispersion in an unsaturated field soil. Water Resour. Res. 35 (10), 3049–3060.

Forrer, I., Papritz, A., Kasteel, R., Flühler, H., Luca, D., 2000. Quantifying dye tracers in soil profiles by image processing. Eur. J. Soil Sci. 51, 313–322.

German-Heins, J., Flury, M., 2000. Sorption of brilliant blue FCF in soils affected by pH and ionic strength. Geoderma 97, 87–101.

Ghodrati, M., Jury, W.A., 1990. A field study using dyes to characterize preferential flow of water. Soil Sci. Soc. Am. J. 54 (6), 1558–1563.

Hatano, R., Booltink, H.W.G., 1992. Using fractal dimensions of stained flow patterns in a clay soil to predict bypass flow. J. Hydrol. 135, 121–131.

Hatano, R., Booltink, H.W.G., 1998. Using fractal dimensions of stained flow patterns in a clay soil to predict bypass flow. In: Baveye, P., Parlange, J.-Y., Stewart, B.A. (Eds.), Fractal in Soil Science, pp. 261–291.

Hatano, R., Kawamura, N., Ikeda, J., T., S., 1992. Evaluation of the effect of morphological features of flow paths on solute transport by using fractal dimensions of methylene blue staining pattern. Geoderma 53, 31–44.

Ju, S.-H., Kung, K.-J.S., 1997. Steady-state funnel flow: its characteristics and impact on modeling. Soil Sci. Soc. Am. J. 61 (2), 416–427.

Kasteel, R., Vogel, H.-J., Roth, K., 2002. Effect of non-linear adsorption on the transport behaviour of brilliant blue in a field soil. Eur. J. Soil Sci. 53, 231–240.

Ketelsen, H., Meyer-Windel, S., 1999. Adsorption of brilliant blue FCF by soils. Geoderma 90, 131–145.

Kung, K.-J.S., 1993. Laboratory observation of funnel flow mechanisms and its influence on solute transport. J. Environ. Qual. 22 (1), 91–102.

Logsdon, S.D., Nachabe, M.H., Ahuja, L.R., 1996. Macropore modeling: state of the science. Information Series, vol. 86. Water Resources Research Institute, Colorado State University, Fort Collins.

McBratney, A.B., Moran, C.J., Stewart, J.B., Cattle, S.R., Koppi, A.J., 1992. Modifications to a method of rapid assessment of soil macropore structure by image analysis. Geoderma 53, 255–274.

McIntosh, J., McDonnell, J.J., Peters, N.E., 1999. Tracer and hydrometric study of preferential flow in large undisturbed soil cores from the Georgia Piedmont, USA. Hydrol. Process. 13, 139–155.

Ogawa, S., Baveye, P., Boast, C.W., Parlange, J.-Y., Steenhuis, T., 1999. Surface fractal characteristics of preferential flow patterns in field soils: evaluation and effect of image processing. Geoderma 88 (3), 109–137.

Perillo, C.A., Gupta, S.C., Nater, E.A., Moncrief, J.F., 1998. Flow velocity effects on the retardation of FD&C Blue no. 1 food dye in soil. Soil Sci. Soc. Am. J. 62, 39–45.

Perillo, C.A., Gupta, S.C., Nater, E.A., Moncrief, J.F., 1999. Prevalence and initiation of preferential flow paths in a sandy loam with argillic horizon. Geoderma 89, 307–331.

Peterson, C.T., Hansen, S., Jensen, H.E., 1997. Depth distribution of preferential flow patterns in a sandy loam soil as affected by tillage. Hydrol. Earth Syst. Sci. 4, 769–776.

Richards, J.A., 1986. Remote Sensing Digital Image Analysis. Springer. 281 pp.

Ringrose-Voase, A.J., 1990. One dimensional image analysis of soil structure: I. Principles. J. Soil Sci 41, 499–512.

Ritsema, C.J., Dekker, L.W., 1993. Preferential flow mechanism in a water repellent sandy soil. Water Resour. Res. 29 (7), 2183–2193.

Serra, J., 1988. Image Analysis and Mathematical Morphology, vol. 1. Academic Press, San Diego.

Soille, P., 1999. Morphological Image Analysis—Principles and Applications. Springer, Berlin.

Vanderborght, J., Gähwiller, P., Flühler, H., 2002. Identification of transport processes in soil cores using fluorescent tracers. Soil Sci. Soc. Am. J. 66 (3), 774–787.

van Ommen, H.C., et al., 1989. Experimental assessment of preferential flow paths in a field soil. J. Hydrol. 105, 253–262.

Wang, Z., Lu, J., Wu, L., Harter, T., Jury, W.A., 2002. Visualizing preferential flow paths using ammonium carbonate and a pH indicator. Soil Sci. Soc. Am. J. 66, 347–351.

Weibel, E.R., 1979. Stereological Methods. Practical Methods for Biological Morphometry, vol. 1. Academic Press, London.

Weiler, M., 2001. Mechanisms Controlling Macropore Flow During Infiltration-Dye Tracer Experiments and Simulations ETHZ, Zürich, Switzerland. 151 pp.

Weiler, M., Naef, F., 2003a. An experimental tracer study of the role of macropores in infiltration in grassland soils. Hydrol. Process. 17 (2), 477–493.

Weiler, M., Naef, F., 2003b. Simulating surface and subsurface initiation of macropore flow. J. Hydrol. 273 (1–4), 139–154.